Johanna Sprenger*, Maximilian Neidhardt, Sarah Latus, Sarah Grube, Martin Fischer, and Alexander Schlaefer

Surface Scanning for Navigation Using High-Speed Optical Coherence Tomography

https://doi.org/10.1515/cdbme-2022-0016

Abstract: Medical interventions are often guided by optical tracking systems and optical coherence tomography has shown promising results for markerless tracking of soft tissue. The high spatial resolution and subsurface information contain valuable information about the underlying tissue structure and tracking of certain target structures is in principle possible. However, the small field-of-view complicates the selection of suitable regions-of-interest for tracking. Therefore, we extend an experimental setup and perform volumetric surface scanning of target structures to enlarge the field-of-view. We show that the setup allows for data acquisition and that precise merging of the volumes is possible with mean absolute errors from 0.041 mm to 0.097 mm.

Keywords: Optical Coherence Tomography, Surface Scanning, Volume Stitching, Tracking, Image Guidance

1 Introduction

Image guidance can support medical interventions based on different optical tracking systems. Optical coherence tomography (OCT) allows to acquire volumetric data with high spatial and temporal resolution showing surface features and subsurface information from tissue samples. Therefore, Schlüter et al. [1, 2] consider an OCT system with high volume acquisition rate for tracking. The approach enables markerless tissue tracking in a contactless manner and without radiation exposure. However, the small field-of-view (FOV) limits the localization and selection of suitable target regions for tracking.

Previous work considered volume stitching to merge several overlapping OCT volumes to obtain larger surface scans from the regions-of-interest (ROI). Different systems have been proposed to acquire the data, such as the integration of OCT into a microscope [3] or by mounting an OCT scanhead to a robot [4]. Rajput et al. [5] proposed a registration between OCT and Kinect camera to acquire surface scans and

*Corresponding author: Johanna Sprenger, Institute of Medical Technology and Intelligent Systems, Am Schwarzenberg-Campus 3, Hamburg, Germany, johanna.sprenger@tuhh.de

Maximilian Neidhardt, Sarah Latus, Sarah Grube, Martin Fischer, Alexander Schlaefer, Institute of Medical Technology and Intelligent Systems, Hamburg, Germany

Dahroug et al. [6] estimate the sample pose in an OCT frame with a principal component analysis framework. Various methods for merging the volumes have been proposed, Laves et al. [7] investigated for example 3D optical flow, and also different anatomical sites, such as the bladder [8] have been considered.

However, most of these studies focused on a precise alignment of the volumes and considered OCT data with high spatial sampling rates. When acquiring data with a scanhead, a higher spatial sampling results in a lower temporal sampling rate, thus extending the recording times for each volume and also lowering the tracking speed. In this work, we focus on integrating surface scanning into the OCT tracking setup by Schlüter et al. [1, 2] to enable the localization and selection of suitable targets for tracking. We investigate to what extent we can merge surface scans from single overlapping volumes to obtain scans from larger ROIs. The setup is optimized for high-speed tracking and lower spatial sampling rates are considered to enable higher volume acquisition rates. Hence, the process to align the volumes during volume stitching is more challenging as fewer features are present in the data but on the other hand, there are also less motion artifacts in the volumes. Initially, we acquire OCT volumes of different phantoms by scanning overlapping FOVs. We implement a geometric volume stitching approach and a combination of geometric prealignment with correlation based refinement of volume positioning to merge the single volumes to surface scans. We compare both approaches and evaluate the accuracy of the generated surface scans by comparing the real geometric structures to the scans. Furthermore, we evaluate different scanning regions for the occurrence of lens distortions in the setup. We can show that data acquisition and precise volume stitching is possible.

2 Material and Methods

2.1 Experimental Setup

Our experimental setup is based on a swept-source OCT system (OMES, Optores Germany) with an A-scan rate of $1.59\,\mathrm{MHz}$ and infrared light with a center frequency of $1315\,\mathrm{nm}$. A scanhead is connected to the OCT system to acquire volumetric data with $116\times116\times480$ voxels and an

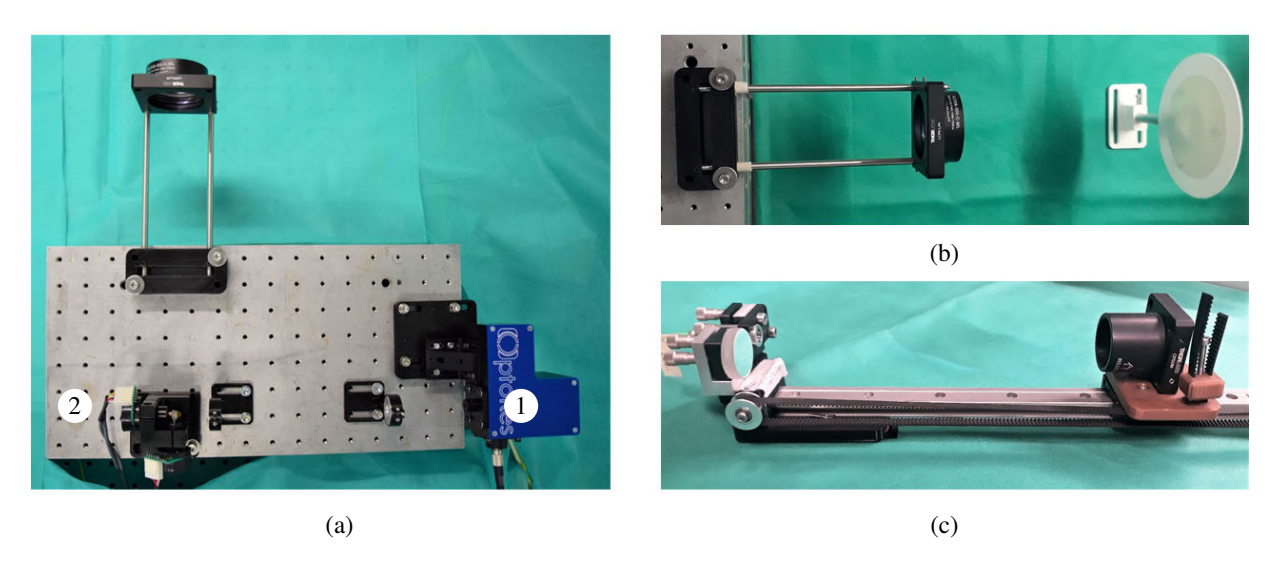


Fig. 1: Our experimental setup (a) is based on an OCT system connected to a scanhead (1) for volumetric imaging. The light is guided to a stage with galvo-mirrors (2) and used to scan targets (b) in the lateral directions. The motorized reference arm (c) is used to scan the target in the axial direction and keep the target surface in the OCT FOV.

acquisition rate of about $94\,\mathrm{Hz}$. The FOV is approximately $5\times5\times3.5\,\mathrm{mm}^3$ with a lateral pixel spacing of about $0.04\,\mathrm{mm}$. The light is guided to an additional stage with galvanometer mirrors (galvos) and focused through an achromatic lens with $50\,\mathrm{mm}$ diameter to move the FOV in the lateral scanning directions (x- and y-direction) over the target by the galvo stage. Furthermore, we employ a motorized reference arm to adapt the OCT FOV in the axial direction (z-direction). The setup was first described for markerless tissue tracking [1], similar as shown in Figure 1.

2.2 Data Acquisition

We obtain OCT volumes by connecting a scanhead to the OCT system and use the motorized galvo stage to move the OCT FOV in the lateral directions to scan larger ROIs. Initially, we evaluate the translation between motor steps and voxels by positioning a marker of known geometric size in the OCT FOV and determine the motor steps shifts in the three dimensions. During the scanning process, we move the galvos to predefined positions in the lateral directions and maintain an overlap between the volumes for later alignment. The FOV is shifted by a third of the OCT's FOV size between neighboring positions. At each position in the lateral directions, the motorized reference arm is moved in a certain range in the axial direction to detect the surface and ensure the target is visible in the FOV. We store the OCT volumes along with the 3D motor position to perform a pre-alignement of the volumes based on the geometric positions.

2.3 Calibration

A marker is placed in the OCT's FOV and the galvos and the motorized reference arm are moved to different positions to induce motion in the OCT FOV to perform a calibration. We perform a segmentation of the marker in the volumes and determine the 3D position in pixel coordinates. The marker and galvo positions are converted to millimeter and a transformation is determined by solving

$$\min_{\mathbf{R}, \mathbf{t}} \sum_{i=1}^{n} \left\| (\mathbf{R}g_i + \mathbf{t}) - p_i \right\|^2 \tag{1}$$

with the galvo positions g_i and the marker coordinates p_i based on Arun et al. [9] to obtain the rotation \mathbf{R} and translation \mathbf{t} . Note, that we only calibrate in the OCT FOV and not the whole scanning area.

2.4 Volume Stitching

We use two methods for volume stitching. First, we perform a geometric volume stitching that we have also considered in a previous work [4]. The 3D motor positions are used to position the overlapping volumes in the larger surface scan. For this purpose, the shifts in the motor positions are transferred to pixel shifts. The lateral positions are precisely determined based on the galvo motor positions and the axial alignment is performed by detecting the surface in the OCT scan which has the highest intensity.

The second method is implemented to detect misalignments in the geometric approach and further improve the pre-

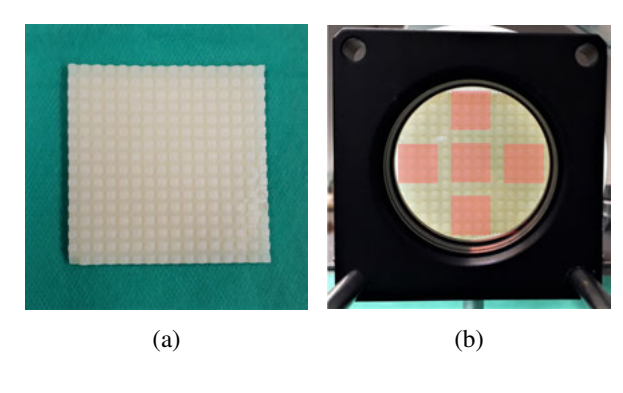


Fig. 2: The cubicboard phantom (a) and the lens with the different scanning areas (b).

cision of the volume alignment. Inherently, using 3D data for alignment of the volumes seems more beneficial, but due to the comparably low spatial spacing of the scans, we focus on a combination of 3D data and 2D maximum intensity projections from the volumes. The motion shifts in the 3D and 2D data are estimated via a cross-correlation. The refinement for the lateral directions is estimated as the average of 3D and 2D motion and the refinement in the axial direction is based on the 3D motion. Note, that we acquire scans with lower spatial spacing to obtain a high temporal resolution during scanning.

Additionally, an intensity blending is applied by weighting the voxels close to the volume border with a logarithmic scaling. The volumes are then aligned with overlapping edges.

2.5 Experiments

Initially, we perform surface scans of a 3D-printed cubicboard phantom in the center of the lens to evaluate the two different methods. The phantom is visualized in Figure 2a with cubes of size $2.2 \times 2.2 \times 1 \,\mathrm{mm}^3$. The evaluation is performed by segmenting the cubes in the merged surface scan and comparing the size in voxels c_i to the real cube's size o_i after transforming from voxel to millimeter [4]. We calculate the mean absolute error

$$MAE = \frac{1}{N} \sum_{i=1}^{N} |c_i - o_i|$$
 (2)

for N cubes for comparison. To investigate if scanning in the periphery of the lens leads to distortions, we use the same cubicboard phantom and perform surface scans at different positions to cover the edges of the lens. A visualization of the scanning zones is shown in Figure 2b. We perform scans in the center of the lens and at four positions on top, below, to the right and to the left of the center. The scans are merged with the correlation method and the previously described evaluation scheme is applied.

Tab. 1: Comparison between geometric volume merging and additional alignment based on correlation.

method	x in [mm]	y in [mm]	z in [mm]
geometric correlation	$\begin{array}{c} 0.061 \pm 0.054 \\ 0.075 \pm 0.053 \end{array}$	$\begin{array}{c} 0.073 \pm 0.054 \\ 0.062 \pm 0.048 \end{array}$	$\begin{array}{c} 0.053 \pm 0.074 \\ 0.050 \pm 0.071 \end{array}$

Tab. 2: Results for volume merging from different scanning positions at the lens.

scanning area	x in [mm]	y in [mm]	z in [mm]
center	0.069 ± 0.043	0.077 ± 0.056	0.074 ± 0.040
top	$\textbf{0.053} \pm \textbf{0.049}$	0.097 ± 0.052	0.050 ± 0.048
bottom	$\textbf{0.070} \pm \textbf{0.036}$	$\textbf{0.088} \pm \textbf{0.036}$	$\textbf{0.046} \pm \textbf{0.031}$
right	0.079 ± 0.067	0.049 ± 0.044	0.084 ± 0.092
left	0.041 ± 0.034	$\textbf{0.094} \pm \textbf{0.061}$	$\textbf{0.057} \pm \textbf{0.053}$

3 Results and Discussion

Firstly, we evaluate the two proposed methods based on a surface scan from the cubicboard acquired at the center of the lens. The resulting mean absolute errors for the three dimensions are reported in Table 1 for a scan of size 8×8 volumes. The errors are similar for both methods, in the range from $0.061\,\mathrm{mm}$ to $0.075\,\mathrm{mm}$. The results from the geometric approach are slightly better in the lateral x-direction and the results from the pre-aligned correlation are slightly better in y-direction. Considering the lateral pixel spacing of roughly $0.04\,\mathrm{mm}$, the errors are in the range of 1-2 voxels. The error values for the axial direction are slightly smaller.

Secondly, we evaluate the peripheral areas of the lens for the occurrence of distortions. The scanning areas are shown in Figure 2b and consist of 6×6 volumes each. The pre-aligned correlation method was applied for volume merging and the resulting errors are reported in Table 2. The errors for the center region are similar to the previously reported values for the larger scan from the cubicboard. The results for the peripheral scanning areas at the lens are comparable. Considering the errors in the lateral directions, the values in y-direction are slightly higher in four of the scanning areas. But the differences are only in subpixel accuracy scale and probably due to fluctuations in scanning and the evaluation scheme. There are no noticeable differences between the scanning areas, leading to the assumption that no lens distortions occur in the scanned area or that possible distortions only have a small not measurable impact below the resolution of the mean absolute error from volume stitching.

Figure 3a shows the top view of a scan from the cubicboard phantom as used for the evaluation and Figure 3b shows a different phantom with circles engraved in a surface.

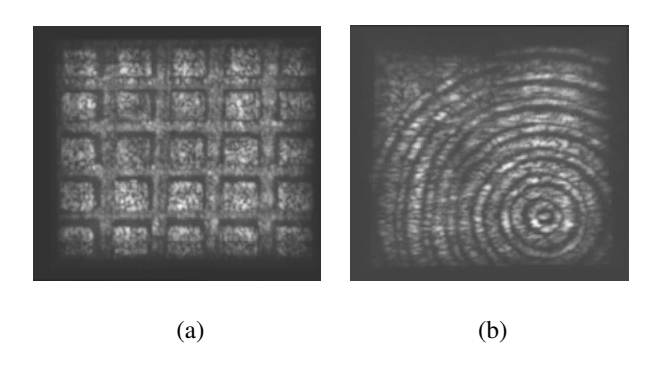


Fig. 3: Top view of surface scans from two different phantoms, the cubicboard phantom (a) was used for evaluation. The second phantom consists of differently sized circles (b).

The circle phantom is better suited to detect small shifts in between the volumes. Both scans are precisely aligned. However, some intensity variations are visible which can occur due to different working distances to the sample surface during volume acquisition. The precise alignment of the volumes is of importance for succeeding processing of the surface scans. Anatomical details can be present but edges and shifts between neighbouring scans should be avoided as they can impede automated processing, e.g. to find suitable regions for tracking. We acquire data with a larger FOV to enable scanning of larger areas but the setup generally allows for a smaller FOV resulting in a higher lateral spacing when acquiring volumes with the same amount of A-scans.

4 Conclusion

We have successfully integrated surface scanning into an experimental setup for OCT tracking and have shown that precise merging of the volumes is possible. Furthermore, we evaluated the peripheral scanning regions for distortions in the volumes. While we have so far focused on precise scanning, the setup generally allows for high-speed volume acquisition and future work will focus on speeding up the scanning process to allow scanning of arbitrary surfaces in short times. Considering moving targets, e.g. patients, a fast scanning is of importance to avoid motion artifacts in the data. Additionally, different FOV sizes should be investigated along with different numbers of A-scans per volume to analyze the trade-off between high spatial and temporal sampling, especially in the context of the number of volumes acquired for a surface scan. The calibration process can also be extended to cover the whole scanning area and a more precise positioning in the axial direction before data acquisition could compensate for intensity variations based on the working distance. In summary, the surface scans allow for extending the target area and enable the localisation of suitable structures for tracking when using OCT for image guidance.

Author Statement

Research funding: This work is partially supported by the i^3 initiative of the Hamburg University of Technology. Conflict of interest: Authors state no conflict of interest. Informed consent: Informed consent has been obtained from all individuals included in this study. Ethical approval: No ethical approval was required.

References

- [1] Schlüter M, Glandorf L, Sprenger J, Gromniak M, Neidhardt M, Saathoff T, Schlaefer A. High-speed markerless tissue motion tracking using volumetric optical coherence tomography images. In 2020 IEEE 17th International Symposium on Biomedical Imaging (ISBI) 2020; 1979-1982
- [2] Schlüter M, Glandorf L, Gromniak M, Saathoff T, Schlaefer, A. Concept for markerless 6D tracking employing volumetric optical coherence tomography. Sensors 2020, 20(9), 2678.
- [3] Finke M, Kantelhardt S, Schlaefer A, Bruder R, Lankenau E, Giese A, Schweikard A. Automatic scanning of large tissue areas in neurosurgery using optical coherence tomography. The International Journal of Medical Robotics and Computer Assisted Surgery 2012, 8(3), 327-336.
- [4] Sprenger J, Saathoff T, Schlaefer A. Automated robotic surface scanning With optical coherence tomography. 2021 IEEE 18th International Symposium on Biomedical Imaging (ISBI). IEEE, 2021.
- [5] Rajput O, Antoni ST, Otte C, Saathoff T, Matthäus L, Schlaefer A. High accuracy 3D data acquisition using co-registered OCT and kinect. In 2016 IEEE International Conference on Multisensor Fusion and Integration for Intelligent Systems (MFI), 2016, (pp. 32-37). IEEE.
- [6] Dahroug B, Tamadazte B, Andreff N. PCA-based visual servoing using optical coherence tomography. IEEE Robotics and Automation Letters. 2020 Feb 28;5(2):3430-7.
- [7] Laves MH, Kahrs LA, Ortmaier T. Volumetric 3D stitching of optical coherence tomography volumes. Current Directions in Biomedical Engineering. 2018 Sep 1;4(1):327-30.
- [8] Lurie KL, Ellerbee AK. Volumetric mosaicing for optical coherence tomography for large area bladder wall visualization. InPhotonic Therapeutics and Diagnostics X 2014 Mar 4 (Vol. 8926, p. 89261P). International Society for Optics and Photonics.
- [9] Arun KS, Huang TS, Blostein SD. Least-squares fitting of two 3-D point sets, in IEEE Transactions on Pattern Analysis and Machine Intelligence, vol. PAMI-9, no. 5, pp. 698-700, Sept. 1987